Creating 3D Objects with Integrated Electronics via Multiphoton Fabrication In Vitro and In Vivo

Sara J. Baldock, Punarja Kevin, Garry R. Harper, Rebecca Griffin, Hussein H. Genedy, M. James Fong, Zhiyi Zhao, Zijian Zhang, Yaochun Shen, Hungyen Lin, Catherine Au, Jack R. Martin, Mark D. Ashton, Mathew J. Haskew, Beverly Stewart, Olga Efremova, Reza N. Esfahani, Hedley C. A. Emsley, John B. Appleby, David Cheneler, Damian M. Cummings, Alexandre Benedetto,* and John G. Hardy*

3D objects with integrated electronics are produced using an additive manufacturing approach relying on multiphoton fabrication (direct laser writing, (DLW)). Conducting polymer-based structures (with micrometer-millimeter scale features) are printed within exemplar matrices, including an elastomer (polydimethylsiloxane, (PDMS)) have been widely investigated for biomedical applications. The fidelity of the printing process in PDMS is assessed by optical coherence tomography, and the conducting polymer structures are demonstrated to be capable of stimulating mouse brain tissue in vitro. Furthermore, the applicability of the approach to printing structures in vivo is demonstrated in live nematodes (*Caenorhabditis elegans*). These results highlight the potential for such additive manufacturing approaches to produce next-generation advanced material technologies, notably integrated electronics for technical and medical applications (e.g., human-computer interfaces).

1. Introduction

Advances in the manufacturing and miniaturization of electronics and components thereof (computers, microprocessors, transistors, etc.) have revolutionized our lives with the ubiquity of electronic devices in our daily lives and underpin the economic success of countries across the world.[1] Electronic technologies employ conductors/semiconductors to fulfill specific roles within manufactured devices, and for a variety of reasons organic conductors and semiconductors (e.g., derivatives of carbon nanotubes, graphene, conjugated polymers, etc.) are playing an increasingly important role in these devices (e.g., in flexible/printable electronics, electronic interfaces for the body, etc.).[2–19]

S. J. Baldock, P. Kevin, G. R. Harper, R. Griffin, H. H. Genedy,
M. J. Fong, M. D. Ashton, M. J. Haskew, J. G. Hardy
Department of Chemistry
Lancaster University
John Creed Avenue, Lancaster LA1 4YB, UK
E-mail: j.g.hardy@lancaster.ac.uk
R. Griffin, C. Au, J. R. Martin, A. Benedetto
Division of Biomedical and Life Sciences
Lancaster University
Tower Avenue, Lancaster LA1 4YQ, UK
E-mail: a.benedetto@lancaster.ac.uk
Z. Zhao, Z. Zhang, Y. Shen
Department of Electrical Engineering and Electronics
University of Liverpool
Liverpool L69 3GJ, UK

H. Lin, D. Cheneler
School of Engineering
Lancaster University
Gillow Avenue, Lancaster LA1 4YW, UK
B. Stewart
School of Chemistry and Biosciences
University of Bradford
Bradford BD7 1DP, UK
O. Efremova
NeuDrive Ltd.
Daresbury Laboratory
Sci-Tech
Keckwick Lane, Daresbury, Warrington WA4 4AD, UK
R. N. Esfahani
The Manufacturing Technology Centre
Ansty Business Park
Coventry CV7 9JU, UK
H. C. A. Emsley
Lancashire Teaching Hospitals NHS Trust
Royal Preston Hospital
Sharoe Green Lane, Preston PR2 9HT, UK

Integrated circuits used in electronics worldwide (e.g., for applications including, but not limited to, amplifiers, logic units, sensors, etc.) are typically mass-produced in a layer-by-layer approach.[1] The manufacture of 3D objects with integrated electronics has become an area of intense research interest with a view to the development of flexible electronics.[3,7,11,20,21,22]

There are a number of U.S. Food and Drug Administration (FDA)-approved medical devices capable of electrical stimulation within the body, including cardiac pacemakers, bionic eyes, bionic ears, and electrodes for deep brain stimulation; all of which are designed for long-term implantation (via a technically challenging surgical procedure).[3] Conducting polymers (e.g., polyaniline, polypyrrole [PPY], poly(3,4-ethylenedioxythiophene) [PEDOT]) can electrically stimulate cells in vitro, and have proven well-tolerated when implanted into small mammals (e.g., mice, rats, and rabbits). Their immunogenicity profile is comparable to FDA-approved non-conductive polymers such as poly(lactic-co-glycolic acid) (PLGA), supporting their safety in vivo; these preclinical studies suggest that conducting polymer-based biomaterials are promising for eventual clinical translation.[23]

Furthermore, the tunable properties of conducting polymers (CPs, e.g., derivatives of polyaniline, PPY, and polythiophene) make them versatile components of electronic devices.[24] Various methods can be used for CP preparation (including solution phase synthesis, solid phase synthesis, electropolymerization, vapor deposition, or photopolymerization), offering opportunities for inclusion in most standard electronic device manufacturing processes.[25,26]

There are a number of approaches to preparing flexible bioelectronics,[3,11,27–30] often involving layer-by-layer processing,[31] however, novel photochemical techniques are under development (e.g., for ion conductive hydrogels).[32] Such approaches are effective routes to functional electronic devices and the ability to prepare electronics with de-novo-designed architectures via printing is appealing for technical and medical applications. It is possible to employ additive manufacturing (AM) techniques to produce components for electronic applications,[33,34] for example printing CP-based materials using various methods, including extrusion, inkjet printing, photopolymerization, rotary printing, screen printing, and so on.[35]

H. C. A. Emsley, J. B. Appleby
Lancaster Medical School
Health Innovation One
Sir John Fisher Drive
Lancaster University
Lancaster LA1 4AT, UK

D. Cheneler, J. G. Hardy
Materials Science Institute
Lancaster University
Lancaster LA1 4YW, UK

D. M. Cummings
Department of Neuroscience
Physiology and Pharmacology
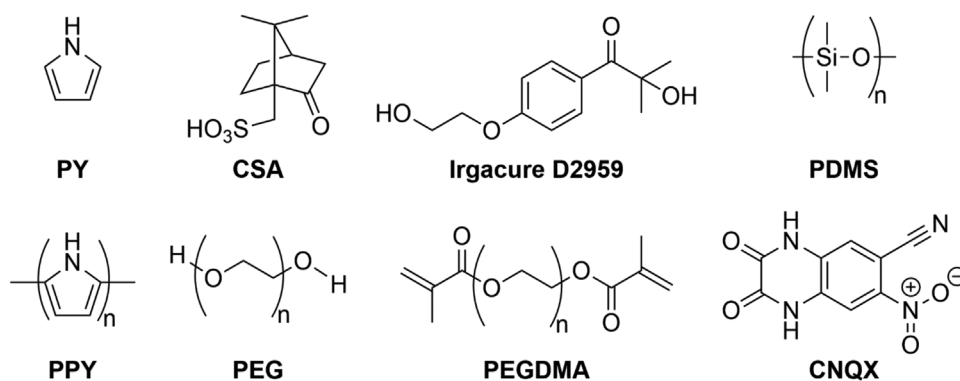University College London
London WC1E 6BT, UK

A. Benedetto
Centre for Ageing Research
Lancaster University
Lancaster LA1 4YQ, UK

Multiphoton fabrication is an AM approach that potentially allows the manufacture of bespoke architectures with features on various length scales (i.e., nm μm^{-1} to mm scale) either free-standing (e.g., on glass) or embedded within a matrix of another substance (e.g., in Nafion sheets), useful for the production of integrated circuits[36,37] within the complex geometry of 3D printed parts and addressing limitations in applications where a high level of customization is required.[38–40] Herein, the concept was applied to printing conducting polymer (PPY)-based structures[41] within insulators (e.g., PDMS and shape memory polymers [SMPs][42–45]) in vitro and in vivo in transparent nematode worms (*Caenorhabditis elegans*). The functionality of the structures for biomedical applications was exemplified by using the conducting polymer-based structures embedded in PDMS to stimulate electrical activity in nerve tissue (an in vitro brain tissue paradigm). Such 3D printed electronics may facilitate fundamental studies (in vitro and in vivo) of the nervous system and its connectivity (e.g., enabling precise, long-term, and continuous monitoring of patients over their lifetimes); or indeed the production of bioelectronic devices capable of continuous monitoring and modulation of neural activity. A particularly exciting aspect of the 3D-printed electrodes is the potential to tailor electrode array designs specific to patients and their needs. Integration with artificial intelligence and machine learning approaches[46–49] for the development and operation of smart neuromodulation systems and/or human-computer interfaces (potentially also useful for the gaming and virtual reality industries), would further support the transition from industry 4.0 (technology-driven manufacturing) to industry 5.0 (human-centric design and resilient/sustainable bespoke manufacturing).[50–52]

2. Results and Discussion

2.1. Additive Manufacturing of Conducting Polymer-Based Electronics Integrated in 3D Objects In Vitro

A variety of computational approaches (with different lengths and time scales) can be applied to study materials and facilitate the development/production of advanced functional materials for a broad spectrum of technical and medical applications.[53,54] The integration of computational materials engineering approaches in workflows applies the Materials Genome Initiative concept for accelerating the discovery, manufacture, and deployment of advanced materials which underpin millions of jobs worldwide in an area of high economic growth.[55,56] We envision in silico approaches supporting the additive manufacturing of advanced functional materials for bioelectronic applications (e.g., in ink formulation, additive manufacturing process optimization, etc.). Understanding the cytocompatibility/biocompatibility of materials is important when contemplating their potential for various applications and their end-of-life.[57–59] In silico toxicity screening has been developed to predict negative outcomes in various organisms (mammals, humans, etc.) and in the environment if exposed to molecules (e.g., those being developed for agriculture/healthcare markets);[60–66] the large datasets offer a more reliable/robust method of assessing toxicity than individual measures such as

**ADVANCED
SCIENCE NEWS**
www.advancedsciencenews.com

**ADVANCED
MATERIALS
TECHNOLOGIES**
www.advmattechnol.de

Figure 1. Structures of chemicals used for fabrication of CSA-doped PPY in/on PDMS films and in vitro validation of function as electrodes capable of stimulating brain tissue.
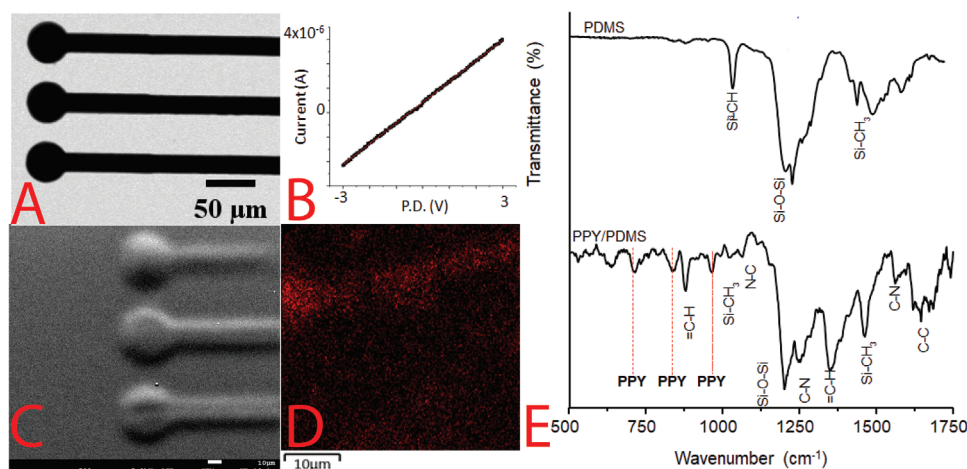
the median lethal dose (LD50)[67] which are prone to variations between testing factors (administration method, environmental factors, genetics, species, etc.),[68] and moreover, conform to the most important principles of processes involving animals in ethically sound research and development (i.e., replacement, reduction, and refinement, the 3Rs).[61,69–71] We have previously employed Derek Nexus and Sarah Nexus (Derek Nexus is an expert rule-based system to identify structural alerts for several endpoints and Sarah Nexus is a statistical-based model focused on mutagenicity only) to assess the biocompatibility of biomaterials,[72–74] including PDMS,[75] which is popular in biomedical applications (e.g., coatings of cochlear implants) due to its flexibility and transparency.[7,76–78] However, PDMS contains ether/organosilicon bonds which may be hepatotoxic/nephrotoxic,[79–81] it may degrade,[82,83] and its surface chemistry may need to be tuned to minimize biofouling;[84–86] pyrrole (acknowledged in supplier's safety data sheets (SDSs), which are of variable quality, to display a degree of toxicity, with significant variation in LD50 between species and mode of administration), the photoinitiator (irgacure D-2959; SDSs indicating it to be somewhat toxic), and PPY (non-hazardous in supplier's SDSs), which were predicted to be non-sensitizers of skin, and non-mutagenic.[73,87] Here we screen the other components utilized in the printing of PPY-based structures within PDMS (employing ink formulations composed of mixtures of the monomer pyrrole, PY; the photoinitiator (irgacure D-2959), dopant (camphorsulfonic acid, CSA; SDSs indicating it to be corrosive and toxic), and a combination of polyethylene glycol (PEG, 10 kDa; SDSs indicating it to be non-hazardous) and polyethylene glycol dimethyacrylate (PEGDMA, 2 kDa; SDSs variable, often indicated to be an eye irritant, skin sensitizer, and toxic), depicted in **Figure 1**). In silico toxicity screening studies of the ink components (CSA, and PEG, Table S1, Supporting Information) using Derek Nexus (Derek Nexus: 6.0.1, Nexus: 2.2.2) predicted them to be non-sensitizers of skin, and in silico mutagenicity screening studies using Sarah Nexus (Sarah Nexus: 3.0.0, Sarah Model: 2.0) predicted them to be non-mutagenic; by contrast, PEGDMA is predicted to plausibly cause chromosome damage, cause irritation of eyes/skin, be a sensitizer of skin (albeit non-mutagenic). In the case of the PPY electronics integrated in PDMS films, it is possible to contemplate their use as conformable bioelectrodes in vivo (however, the potential for slow degradation of PDMS[82,83] means they may

need to be removed after some time in vivo, pending lifetime assessments), or indeed as bioelectrodes for in vitro studies.

Thin films of PDMS were prepared by spin coating (Table S2, Supporting Information) and swollen with ink formulations composed of mixtures of PY, irgacure D-2959, CSA, PEG, and PEGDMA. A commercially available multiphoton fabrication apparatus (Nanoscribe Photonic Professional GT 700) was used to print structures based on computer-aided design (CAD) models via the polymerization of PY (yielding PPY), enabling the fabrication of conductive structures within and on the surface of the PDMS that would facilitate connection to other devices/objects. Once the multiphoton fabrication process was complete, the substrate was washed with ethanol/water to remove traces of low molecular weight contaminants and dried, yielding prototype electrodes with interconnecting wires based on printed conducting polymer structures (CSA-doped PPY) with feature sizes from micrometer to millimeter scale integrated in PDMS.

The darkly colored printed structures were visible by the eye within the transparent PDMS matrices (an optical microscope image is shown in **Figure 2**A), the conductivity of which was measured using a probe station and observed to be 3.9 ± 0.3 S m^{-1} (Figure 2B). Scanning electron microscopy (SEM) of PPY/PDMS structures (Figure 2C) shows the printed PPY structures emerge from the PDMS matrices, and corresponding energy dispersive X-ray spectroscopy (EDX) spectroscopy of the Kα emission of C of the PPY/PDMS structures (Figure 2D) shows correspondingly enhanced carbon content (red) in the printed PPY structures that emerge from the PDMS matrices (mostly black). Fourier transform infrared (FTIR) spectroscopy confirmed the printed structures were PPY (Figure 2E); the PDMS matrices had characteristic peaks at 789–796 cm^{-1} (–CH$_3$ rocking and Si-C stretching in Si-CH$_3$), 1020–1074 cm^{-1} (Si-O-Si stretching), 1260–1259 cm^{-1} (CH$_3$ deformation in Si-CH$_3$), and the samples with PPY structures in/on the PDMS have additional peaks characteristic of the PPY (C–C stretching at 1560 cm^{-1}, C–N stretching at 1435 cm^{-1}, =C–H in-plane vibration at 1315 cm^{-1}, C–H or C–N in-plane deformations at 1260 and 1280 cm^{-1}, respectively).

The fidelity of the printing process was assessed by comparison of the CAD files of the designed structures and optical coherence tomography (OCT, for setup, see Figure S1, Supporting Information) of the structures actually printed,

**ADVANCED
SCIENCE NEWS**

www.advancedsciencenews.com

**ADVANCED
MATERIALS
TECHNOLOGIES**

www.advmattechnol.de

Figure 2. A) Optical microscope image of an exemplar PPY/PDMS structure (scale bar represents 50 μm). B) FTIR spectra of PDMS, PPY/PDMS structures. C) SEM image of an exemplar PPY/PDMS structure (scale bar represents 10 μm). D) EDX image of an exemplar PPY/PDMS structure, where the intensity of Kα emission of C (red) is mapped relative to the background PDMS (black); the scale bar represents 10 μm. E) FTIR spectra of PDMS and PPY/PDMS.

an example of which for PPY/PDMS structures is depicted in **Figure 3**. For PPY/PDMS structures we observed the fidelity of the printing process in the x–y dimensions to be ≈100 ± 7%, however, in the z-dimension it was much more variable, assessed to be ≈25% for thick structures (desired thickness of 65 μm), whereas ≈540% for thinner structures (desired thickness of 5 μm), see also Figures S2–S5, Supporting Information. The variations in actual versus desired structures are caused by heating of the inks/PDMS matrices during the printing process and absorption of light as the monomers polymerize yielding darkly colored conjugated polymers and should be possible to further optimize. Future optimization of the printing process in an application-/technology-specific fashion will enable the integration of plastic electronics solutions (such as organic thin film transistors and memristors that would allow recording of the action potentials as well as stimulation), printed antennas and batteries for powering and data transmission, which may enable continuous monitoring and modulation.[1]

Field stimulation experiments focusing on a single polymer electrode and its operational environment were simulated using an electromagnetic field solver in ANSYS Electronics
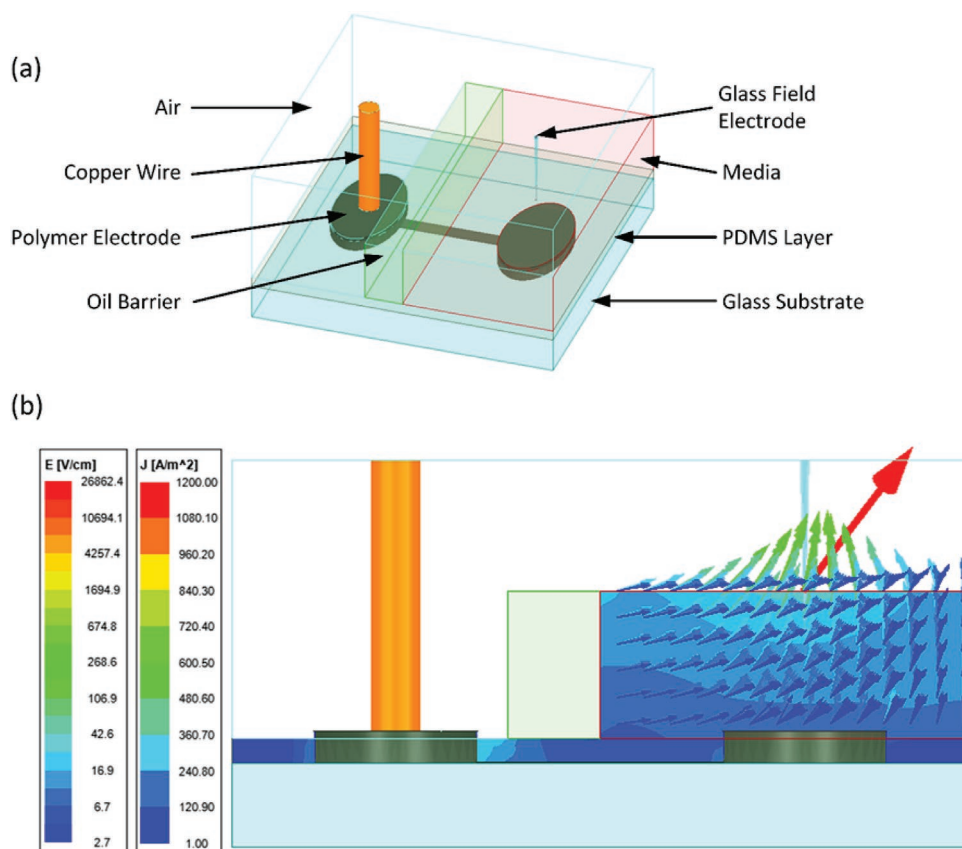
Desktop 2020 R2 using Maxwell 3D with electrical transient solution type (see **Figure 4**). Here, the tissue was simplified to be a homogeneous material with a conductivity of 0.33 S m^{-1}, which is similar to that of mouse brain tissue.[88] These simulations show how the electric field and current density are expected to evolve as the stimulation is applied if there were no cellular activity within the tissue and can be used to optimize experimentation. Simulations show that electric fields established initially between the polymer electrode and glass field electrode upon stimulation result in a flow of charge towards the glass field electrode, as expected. This acts to reduce the electric field gradient within the tissue in accordance with Gauss' law reaching a steady state (under constant voltage excitation) within ≈5 μs.

To demonstrate that the conducting polymer electronics integrated in PDMS can be used as neural interfaces, we used the electrodes to stimulate a slice of mouse brain in vitro. The electrodes were positioned to stimulate the Schaffer collaterals in the stratum radiatum and a single CA1 pyramidal neuron was patch-clamped using standard methodology, permitting CA3–CA1 synapses to be recorded (**Figure 5**). A square potential step of 10 V was applied for 80 μs to the PDMS electrode. While the
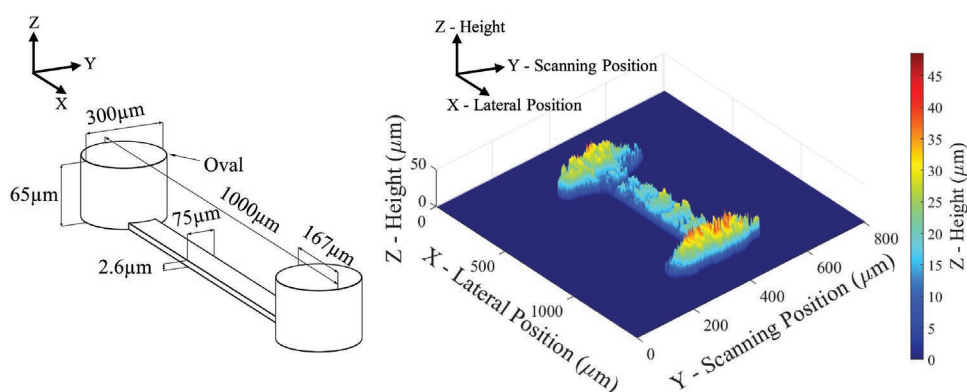
Figure 3. 3D rendering of PPY/PDMS polymer electrode structures. Left) Example CAD structure. Right) Actual structure produced as observed by OCT.

**ADVANCED
SCIENCE NEWS**

www.advancedsciencenews.com

**ADVANCED
MATERIALS
TECHNOLOGIES**

www.advmattechnol.de

Figure 4. a) Schematic of EM field simulation. b) Magnitude of electric field (contour plot) and current density (vector plot) as stimulation is initially applied.
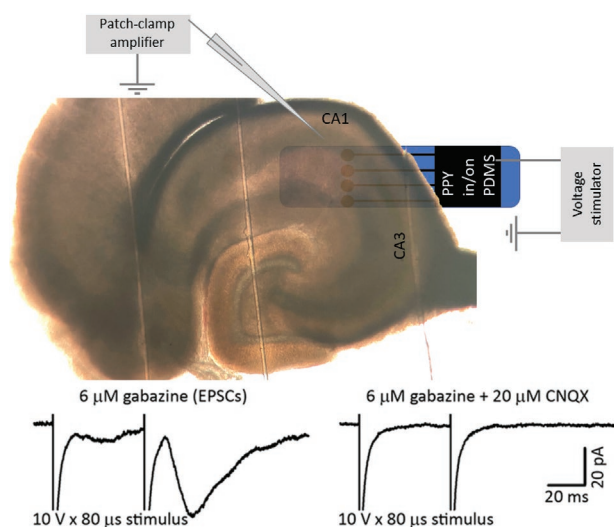
stimulus artifact was wider than that typically obtained with a conventional glass stimulating electrode, a corresponding physiological response was evoked by the PDMS electrode (Figure 5, left trace), indicating that the electrodes interact with the nervous system. Importantly, typical CA3-CA1 synaptic properties were observed, whereby the application of two stimuli at a 50 ms inter-pulse interval resulted in paired-pulse facilitation, that is, the second response was larger than the first, reflective of the low initial probability of presynaptic release of the neurotransmitter glutamate at these synapses. Moreover, as would be expected for excitatory currents in the central nervous system, a competitive antagonist of the postsynaptic α-amino-3-hydroxy-5-methyl-4-isoxazolepropionic acid (AMPA)/kainate class of glutamate receptors, 6-cyano-7-nitroquinoxaline-2,3-dione (CNQX), completely abolished the synaptic response, leaving only the stimulus artifact (Figure 5, right trace), indicating that the evoked responses are physiological and indeed synaptic in nature.

Printed electronics integrated in flexible substrates such as those described herein have significant potential for technical applications (e.g., display technologies) and medical applications (e.g., patient-specific implantable electrodes for interaction with the central/peripheral nervous system). Printing conducting polymer structures integrated in shape-memory polymer-based materials may facilitate the development of switches, nerve cuff electrodes, etc.,[42,89–94] and proof-of-concept

it would be possible to realize such applications was demonstrated by printing PPY structures in/on thin films of an optically transparent SMP (shape-memory polyimide, Figure S6, Supporting Information).[95]

2.2. Additive Manufacturing of Conducting Polymer-Based Electronics Integrated in 3D Objects In Vivo

Researchers have previously generated abiotic conducting polymers using electropolymerization in the vicinity of live cells,[96] or indeed oxidative enzymes present in plants[97–99] and invertebrate *Hydra*,[100] in analogy to the production of natural melanins in a variety of organisms.[101] Multiphoton fabrication has been used to print free-standing conducting polymer structures used as an interface for mouse brain slices in vitro,[41] and to print non-conducting polymer-based hydrogels in the vicinity of live cells in vitro,[102] and *C. elegans*,[103] observing relatively low levels of cytotoxicity over the short timeframe of the experiments. The direct printing of conducting polymer structures directly on/in living organisms would enable real-time repairs of implanted bioelectronic devices and other applications (e.g., miniaturization/customization, precisely controlled reconfiguration of the electronics),[104] however, it has not yet been reported in the literature.[105] To facilitate proof-of-concept that such a technological leap is within reach and it would be

**ADVANCED
SCIENCE NEWS**

www.advancedsciencenews.com

**ADVANCED
MATERIALS
TECHNOLOGIES**

www.advmattechnol.de

Figure 5. Top) Placement of an in vitro hippocampal brain slice on top of a schematic of a PDMS array, such that electrodes contacted presynaptic CA3 axons (Schaffer collaterals). Postsynaptic responses to action potentials evoked in the Schaffer collaterals by a square voltage pulse applied via the PDMS electrodes were recorded from a CA1 pyramidal neuron using a patch electrode in a whole-cell voltage-clamp configuration. Bottom, left) The GABA$_A$ receptor antagonist gabazine was applied to block inhibitory currents, revealing a purely glutamatergic excitatory postsynaptic current (EPSC). Paired stimuli resulted in paired-pulse facilitation; the typical form of short-term plasticity displayed at these synapses. Bottom, right) The glutamatergic nature of the synaptic response was confirmed by the application of an antagonist of AMPA/kainate subtypes of glutamate receptors, CNQX, which abolished the synaptic response, leaving only the stimulus artifact.
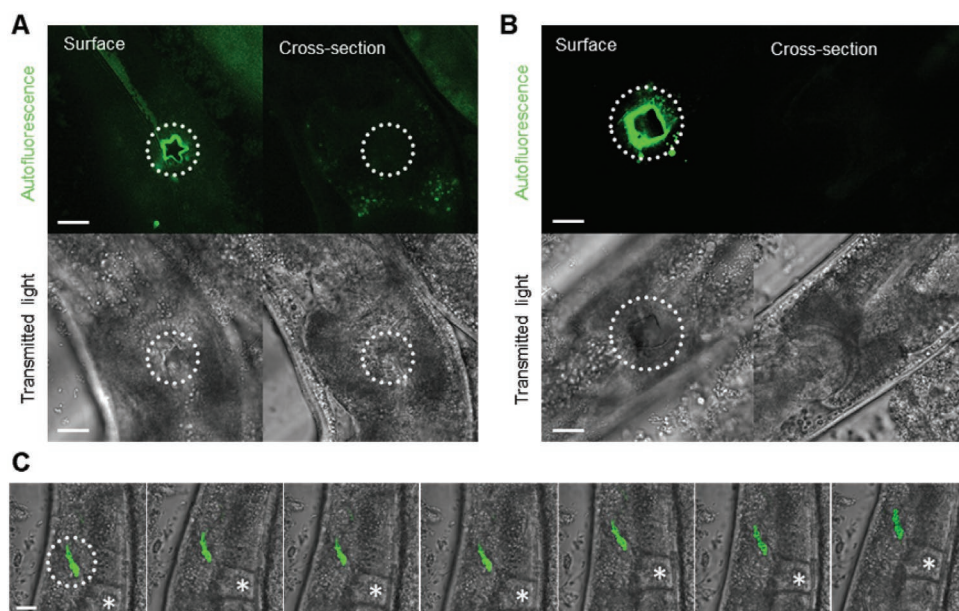
possible to realize such applications, we applied multiphoton fabrication to print PPY-based structures on/in live *C. elegans* (**Figure 6**), which complements reports on printing of non-conductive polymer structures employing near-infrared (NIR) light sources.[106,107] We chose *C. elegans* for ethical reasons, but also for its high sensitivity to heat, desiccation, and physical injury, making it an ideal testing ground for biosafe laser-based in vivo printing approaches in biomedicine. Achieving laser printing on/in live *C. elegans* would require the lowest possible laser power that enables ink polymerization and biocompatible ink components. The PPY-based formulations described earlier were thus first evaluated for *C. elegans* toxicity in order to design a biocompatible ink. While the photo-polymerized ink is inert and non-toxic, future biomedical applications would involve tissue exposure to the unpolymerized mixture prior to in vivo printing. It was thus necessary to determine the toxicity of each individual ink component in the solution. Two toxicity assays were performed to measure 1) acute adult toxicity and 2) chronic developmental toxicity, for various concentrations of each compound. The former involves exposing adult worms to compounds for 24–48 h and relies on the label-free automated survival scoring (LFASS) technique,[108] which exploits the fact that worms fluoresce in blue when they die to pinpoint the median time of death.[109] The latter assesses the timing and duration of *C. elegans*' successive larval stages and ability to reach reproductive age, using a transgenic strain that produces bioluminescence when the worm is metabolically active.[110]

As worms progress through the four larval stages, they feed at increasing rates (commensurate with their size) and produce more bioluminescence. Between larval stages, worms undergo molts during which they cease feeding and appear metabolically quiescent, giving out little bioluminescence. Time-lapse recording of bioluminescence thus enables timing and measurement of developmental stages as bioluminescence rises and falls.

Acute adult toxicity assays revealed that all ink components are acutely toxic at concentrations of 6, 8, and 10 mg mL^{-1} but not below 3 mg mL^{-1} (Figure S7, Supporting Information), while only CSA remained acutely toxic at 4 mg mL^{-1}. Conversely, neither of the compounds showed any strong developmental toxicity across the range of concentrations tested (10 µg mL^{-1} down to 156 ng mL^{-1}), as they all allowed worms to reach adulthood in a timely manner (Figure S8, Supporting Information); although higher doses (2.5–10 µg mL^{-1}) of irgacure, pyrrole, and PEG led to modest developmental shifts (Figure S9, Supporting Information). These results indicated that the PPY ink components in the solution were compatible with in vivo printing when employed at concentrations below 4 mg mL^{-1}. In particular, HA revealed more biocompatible than CSA and was thus chosen as a photoinitiator in the subsequent phases of ink formulation refinement.

Next, to dilute the ink component down to biocompatible concentrations, and because *C. elegans* would not naturally consume the ink alone, ink formulations were mixed with dietary *E. coli* OP50 bacterial paste. As ink dilutes into a bacterial paste is expected to impact printing performance, several ink-to-bacterial paste ratios were tested to determine the lowest ratio compatible with live laser printing. Ink-to-bacterial paste ratios at 1:1 to 1:10 were tested first on polydimethylsiloxane (PDMS)-coated coverslips and the fidelity of intended printed structures was assessed (Figure S10, Supporting Information). While sub-millimetric structures could be printed at 1:10 ink-to-bacterial paste ratios (Figure S10A–C, Supporting Information), resolving 10–30 micron scale structures was only fully achieved with pure ink formulations (Figure S10D–F, Supporting Information).

C. elegans were then exposed to HA-based ink formulations mixed with dietary *E. coli* OP50 bacterial paste at 1:5 ratios as a compromise between biocompatibility and printing resolution. Lower-energy infrared two-photon 3D printing was chosen to reduce phototoxicity while enabling deeper tissue penetration (Figure S11, Supporting Information). Two formulations were tested with subtoxic (3.3 mg mL^{-1}, Figure S11C, Supporting Information) or mildly toxic (6.6 mg mL^{-1}, Figure S11A,B,D, Supporting Information) irgacure concentrations. 6–10 µm size square and star shapes were then printed directly onto the skin and within the gut of live *C. elegans* roundworms (Figure 6). Thanks to the autofluorescence properties of the ink mix, the printed shapes were imaged and localized by confocal fluorescence imaging, demonstrating accurate and well-tolerated printing of polymer on live worms (Figure 6 and Figure S11, Supporting Information). Printing within the moving gut of the worm did not yield the intended shape (Figure 6C). Faster printing could resolve this limitation, which may be achieved by improving the ink formulation photo-curing efficacy, and/or increasing laser power. However, as light propagates within

**ADVANCED
SCIENCE NEWS**

www.advancedsciencenews.com

**ADVANCED
MATERIALS
TECHNOLOGIES**

www.advmattechnol.de

Figure 6. 3D printing of photoresist in live *C. elegans*. A) 6 µm-wide and 10 µm thick star shape printed onto the cuticle of an anesthetized worm's head with a Nanoscribe Photonic GT700, imaged by confocal fluorescence (Zeiss LSM880, Exc. 488 nm, Em. 543 nm, top left) and transmitted light imaging at 40×, without damaging the worm (internal structures intact, right bottom panel). B) 10 µm-wide and 10 µm thick square shape printed onto the cuticle of a worm. A,B) Confocal fluorescence (≈0.8 µm depth *z*-resolution) images of the surface versus cross-section structures are taken 6 µm apart. C) Time series of images taken 1.5 s apart in a fixed field of view, following attempted printing of a star shape inside the posterior gut lumen of a live worm that had absorbed a 1:5 mix of ink/photoresist and bacterial paste. Live worm movements limited printing accuracy leading to the printing of a somewhat irregular shape. Dotted circles indicate the locations of printed structures. Asterisks mark the position of the terminal oocyte. Animals were alive following 3D printing. Scale bars represent 10 µm.

a complex environment (here the body of the worm), printing accuracy and precision also decreases. Corrective strategies employing adaptive optics will thus likely be necessary to circumvent the issue when translating the approach to thicker vertebrate/human tissues; nevertheless, this represents a technological leap from examples of printing non-conductive structures in vivo.[106,107]

2.3. Ethics

The research described in this paper has carefully negotiated the ethically sensitive aspects of the experimentation it entailed. For example, *C. elegans* was chosen as a model organism for the in vivo experimentation because it does not need ethical approval to use. In addition, the toxicity of the compounds used in the 3D printing process occurs on such a small scale that there is a negligible risk of harm to the researchers or the environment. One potential concern is that as future stages of this research progress, there may be a growing scientific case to experiment on more complex organisms (e.g., mice) in vivo, and eventually in humans. Given the novel nature of this technology, some may find the thought of first-in-mammal or first-in-human research to be ethically unsettling. However, if this research did reach more advanced stages that required more complex organisms for experimentation, this process would necessarily follow all the typical required safety, ethical, and legal protocols. This would be no different than the development of a novel medical device or an analogous scientific procedure.

While the research carried out in this study is not particularly ethically contentious, there is nevertheless a need to be aware of the potential for "dual-use dilemmas" to emerge as research progresses and becomes more ethically complex. A dual-use dilemma is an ethical dilemma that occurs when research is undertaken with a beneficial use in mind, however, the researchers also foresee that other users may employ this research in ways that could do harm.[111] When it comes to the scientific research outlined in this paper, the authors do not yet feel that the research has reached a point where it could be deployed in ways that could cause harm. However, if this research maintains a successful trajectory, the potential applications it may have at later stages will grow, and some of these applications may carry the risk of harm if misused. For example, human-computer interfaces could be used to beneficially treat medical patients with neurological conditions; however, such technology could also be used by a bad actor in such a way (e.g., hacking into them to control or obtain information from the device) that negatively affects the privacy and autonomy of the individuals using them.[112–114]

One way to responsibly negotiate future dual-use dilemmas is to take steps to try and identify them in advance and subsequently have researchers work with regulators to creatively design ethical safeguards that can be engineered into and alongside the development of the technologies. For example, one safeguarding procedure may involve keeping key aspects of research knowledge secure (e.g., by withholding it) that would otherwise enable the harmful use of such research. Insofar as possible, researchers will need to endeavor to continue to

**ADVANCED
SCIENCE NEWS**

www.advancedsciencenews.com

**ADVANCED
MATERIALS
TECHNOLOGIES**

www.advmattechnol.de

engage in horizon scanning in relation to future stages of this research in order to identify and address ethical dilemmas in advance.

3. Conclusion

Here we report the application of a multiphoton fabrication process to create 3D objects with integrated electronics: in silico toxicity screening of ink components identifies/confirms likely cytocompatible formulations; 3D printing through light-transmitting materials yields well-resolved conductive micronscale features; stimulation of 3D printed PPY structures interfaced with live brain tissue can induce specific synaptic responses; and it is possible to 3D print PPY structures directly in vivo.

We showcase a range of examples made by this technology-driven manufacturing (industry 4.0) process, including PDMS films and a living organism (*C. elegans*); and highlight potential applications such as electrodes capable of stimulating nerve tissue. We foresee the significant potential for this technique's integration in human-centric design and bespoke manufacturing (industry 5.0) processes of producing bioelectronics for telemedicine, and that this represents a possible roadmap for the broader development of direct-printing of electronic devices for biomedical applications in situ.

Computational approaches (e.g., including in silico toxicity screening, multiscale modeling of electrical/mechanical/physicochemical properties, etc.) will facilitate ink formulation development for the production of 3D objects with integrated electronics, offering insights into the properties (e.g., electrical conductivity) of the conjugated polymers which underpins their function in devices. Simulation of the interactions between oligomers of components in the bioelectronic devices (in this case, PDMS, PEG, and PPY in water, mimicking the hydrated state of the bioelectrodes if used in vitro or in vivo) would offer insight into aggregation/clustering due to intramolecular/intermolecular interactions, and potentially phase separation of polymer phases (e.g., associative phase separation). In the long term, we believe that such an approach may offer insights that accelerate the discovery, manufacture, and deployment of complex composites used in advanced materials technologies generated by additive manufacturing approaches, for example, component selection and composition tuning to achieve optimal properties and device performances.

The potential technical advantages of electronics produced via this technique include (but are not limited to): more accurate targeting (fewer cells stimulated/recorded from) to minimize adverse effects (e.g., tissue damage, immunological reaction/inflammation); increased specificity, efficiency, and effectiveness, with the potential of more simultaneous sites for stimulation or recording with optimized signal to noise ratios. Such properties are clinically relevant in the design of implantable bioelectronic devices. With increasing populations and aging populations worldwide, there are concomitant increases in the number of patients suffering from neurodegenerative conditions (including Parkinson's disease) and other conditions that increase with aging (e.g., epilepsy, strokes), as well as rises in traumatic brain injury. In this context, potential applications of the approach described herein may include: improved

electrodes (smaller, lower morbidity, better tolerated, etc.) for deep brain stimulation (e.g., treating Parkinson's disease, epilepsy, etc.), improved monitoring/diagnosis (e.g., advanced epilepsy work-up to identify epileptogenic focus), novel neuroprosthetics (e.g., for traumatic brain injury), new approaches to monitoring/treatment of (peripheral) neuromuscular disorders (e.g., degenerative muscular and peripheral nerve conditions), and novel approaches to neuromodulation for pain. In short, we foresee the technique described herein as having significant potential for technical and medical applications, with potential economic, environmental, health, and societal impacts.

4. Experimental Section

Materials: Aluminum oxide (basic, Brockmann I, for chromatography, 50–200 μm 60A) was purchased from Acros organics. (±)-Camphor-10-sulfonic acid and PEG (Mn 10 kDa) were purchased from Alfa Aesar. Carl Zeiss Immersol immersion oil, coverslips, and polydimethylsiloxane (PDMS, Dow Sylgard 184 Kit) were purchased from Thermo Scientific. Glue (HERMA GmbH) and Amazon. Unless otherwise stated, everything was purchased from Sigma Aldrich and used as supplied (e.g., PEGDMA Mn 2 kDa, pyrrole, 2-hydroxy-4-(2-hydroxyethoxy)-2-methylpropiophenone (irgacure D-2959)).

PDMS Substrate Preparation: Glass substrates (typically coverslips of ≈170 μm thickness) were cleaned by submersion in acetone (1 min), then isopropanol (1 min), and dried under N_2. Dow Sylgard 184 silicone elastomer curing agent (1.2 g) was added to Dow Sylgard 184 silicone elastomer base (12 g) in a disposable centrifuge tube in the ratio and the mixture was stirred with a spatula and then inverted (10 s, 30 times) to ensure thorough mixing of the two components. The PDMS precursor mixture was placed under vacuum in a vacuum desiccator for 30 min to remove any air bubbles, after which 1 mL of the PDMS precursor mixture was placed on a glass coverslip attached to a spin coater (Laurell WS-650-23NPPB spin coater) by vacuum, the spin coater lid was closed, parameters selected from Table S2, Supporting Information, and the spin coater started, and after completion of the steps the coverslips were placed in an oven (90 °C, ≈3 h) yielding films with a range of thicknesses of PDMS (summarized in Table S2, Supporting Information).

In Silico Toxicity Screening: In silico toxicity screening was carried out using Derek Nexus (v. 6.0.1, Nexus: 2.2.2) and Sarah Nexus (Sarah Nexus: 3.0.0, Sarah Model: 2.0) supplied by Lhasa Limited, Leeds, UK.

Ink Formulation for 3D Printing in/on PDMS: A saturated PY-based ink formulation was prepared composed of pyrrole (1 mL, purified by passage over basic alumina), irgacure D-2959 (250 mg), PEG (10 kDa, 1 mg), PEGDMA (2 kDa, 1 mg), and camphorsulfonic acid (330 mg). The ink was sonicated for ≈25 min in the dark at room temperature to ensure mixing, left to rest for ≈25 min in the dark for any insoluble material to settle, and after which the clear upper layer (saturated with monomer, initiator, and dopant) was used for printing.

Printing in/on PDMS: The PDMS-coated coverslips were mounted onto a Nanoscribe 30 mm coverslip holder made of aluminum with the PDMS-coated side facing downwards. Herma glue was dotted around the edges of the coverslip binding it to the holder and left to dry (10 min). A drop of immersion oil was placed on the glass side of the coverslip. The holder was then flipped so that the PDMS/resist face was upwards and oil face was downwards. A drop of one of the clear ink stock solutions was placed on the substrate and left for 5 min to infiltrate the PDMS. The structures to be printed were designed using the computer-aided design (CAD) package (Fusion360 from AutoCAD:Autodesk) and the structures were exported to the Nanoscribe software (DeScribe) to do the scripting. The Nanoscribe Photonic Professional GT 700 instrument was equipped with a light source (Topica FemtoFiber pro, Er-doped fiber laser of wavelength 780 nm, pulse duration < 150 fs, repetition rate 100 MHz, an aperture of 7.3 mm, a diode voltage of 1.34–5, and 50 mW power at the focus point at 100% power). The Nanoscribe was

controlled by the Nanowrite software (version 1.8.14) and the camera software within the Nanoscribe is AxioVision LE (version 4.8.2.0). The structures were printed on PDMS-coated glass slides using Galvo writing mode by moving beam fixed stage (MBFS) – a fast layer-by-layer writing approach, suitable for micrometer to millimeter scale structures with a computer-controlled piezoelectric scanning stage range $300 \times 300 \times 300\ \mu m^3$. Positioning was achieved using a computer-controlled motor stage, range $100 \times 100\ mm^2$. Laser power and speed for printing on PDMS-coated glass substrates the laser power was $\approx$50–60% and the speed was $\approx$5000 $\mu m\ s^{-1}$. After printing structures, the substrates were washed with water-ethanol and water to remove low molecular weight contaminants, and the structures were dried under N_2.

Electrical Measurements: Direct electrical characterization of the structures was performed using a Keithley 2602B source measure unit, connected to a Wentworth Laboratories SPM197 probe station, with tungsten probes with a 1 μm tip diameter. Each wire was swept in a range from 0 V to +1 V DC. $900 \times 40 \times 8\ \mu m$ CSA-doped conductive wires were fabricated within PDMS using 2PP, with circular pads (75 μm diameter) to aid electrical measurements. The electrical properties of the wires were measured with a source-measure unit connected to a probe station. The wires exhibited linear conductance. Their resistance was calculated to be $R_{PPy} = 570 \pm 50\ k\Omega$. Modeling of the structure, the resistivity of the wires could be estimated using

$$\sigma = \frac{1}{\rho} = \frac{1}{R}\frac{A}{l} \tag{1}$$

where R is the measured resistance of the structure, l is the length of the resistor, and A is the cross-sectional area. The doped PPy structures had $\sigma_{PPy} = 3.9 \pm 0.3\ S\ m^{-1}$.

SEM and EDX Spectroscopy: Samples were mounted on stubs and coated with a layer of gold ($\approx$5 nm, 60 s, 20 mA, 8×10^{-2} mBar) using a Quorum Q150RES sputter coater (Quorum Technologies Ltd., Lewes, UK). Images were obtained using a JEOL JSM-7800F (Field Emission SEM, FE-SEM) fitted with an EDX system (X-Max50, Oxford Instruments, Abingdon, UK) at 10 mm working distance and 10 kV voltage, three measurements were performed per sample and average results were presented.

FTIR Spectroscopy: Infrared spectroscopy was carried out on Agilent Cary 630 FTIR Spectrometer. Spectra were recorded in ATR mode, with a 1 cm^{-1} resolution and 64 scans (corrected for background and atmosphere using OMNIC software supplied with the spectrometer).

OCT: A line-field optical coherence tomography (LF-OCT) system was employed to measure the electrode sample. The LF-OCT can acquire cross-sectional images (B-scan) in a single shot,[115] which could significantly reduce motion-induced image distortion and artifacts. The resolution of the system was 8 μm axially and 17.5 μm laterally, which enables high-resolution tomography and topography imaging. Figure S1, Supporting Information shows the LF-OCT system setup, which used a superluminescent diode (SLED) source to generate low-coherence light centered at 840 nm with 50 nm spectral bandwidth. A beamsplitter (BS) was used to split the optical light into the sample arm and reference arm. Line illumination on the sample was achieved by using a cylindrical lens (CYL) and objective lens (L2) resulting in a focused thin line of $\approx$7 mm. As the setup used a Linnik interferometer configuration, the sample arm used the same optics as the reference arm. The backscattered light from the two arms was recombined at the BS for collection by an imaging spectrograph. By scanning the sample across the y-axis, a stack of raw 2D interferograms at various lateral positions could be acquired by yielding a raw 3D data cube. Even though an LF-OCT system had been demonstrated, without a loss of generality, other OCT variants could also be used such as a spectral-domain OCT[116,117] and full-field OCT,[118] though at longer data acquisition time.

Simulations of Field Stimulation Experiments: CSA-doped PPY electrode structure is defined as in Figure 3 (left) integrated with a PDMS layer (50 μm thick) on a borosilicate glass (relative permittivity 5.5, perfectly insulating) coverslip of $\approx$170 μm thickness. The polymer electrode material was taken as PPY with a conductivity of 3.86 $S\ m^{-1}$. The conductivity of PDMS was taken as $2.4 \times 10^{-14}\ S\ m^{-1}$ and the relative

permittivity as 2.5.[119] Glass field electrodes formed from the pulled borosilicate glass capillary filled with artificial cerebrospinal fluid was assumed to have the same conductivity as the media used in the tissue (0.33 $S\ m^{-1}$). The tip of the glass electrode was positioned 200 μm vertically above the center of the end oval of the polymer electrode. Glass electrode tip opening has a diameter of 1 μm. Tissue and media were held in place by a ring of oil (perfectly insulating) of $\approx$170 μm thickness and 300 μm high (same height as the tissue layer). Voltage was applied to the exposed end of the electrode by copper wire 100 μm diameter (conductivity of 58 MS m^{-1}). Stimulation was a constant voltage (20 V, 20 μs) applied to the copper wire with the exposed end of the media in the glass field electrode being set as ground (experimentally this terminal would be an Ag/AgCl wire connecting back to the amplifier). Mesh consisted of 182 872 tetrahedral elements with a maximum element length of 50 μm on polymer electrode and tissue. Simulated for 20 μs (initial step 0.005 μs, max. step 1 μs).

Brain Slice Preparation and Electrical Stimulation: Transverse hippocampal brain slices were prepared from a 22-day-old C56BL/6J mouse, in accordance with the Animal (Scientific Procedures) Act 1986. Slices of 300 μm were cut and bathed in artificial cerebrospinal fluid (ACSF), containing: NaCl 125 mM, KCl 2.4 mM, NaHCO$_3$ 26 mM, NaH$_2$PO$_4$ 1.4 mM, D-glucose 20 mM, MgCl$_2$ 1 mM, CaCl$_2$ 2 mM, $\approx$315 mOsm L^{-1}, pH 7.4, bubbled with 95% O_2/5% CO_2 continuously superfused at a rate of $\approx$2 mL min^{-1} The stimulating electrode was a PPY contact pad with a PPY wire spanning the gap to another PPY contact to which a copper wire was attached with conductive silver epoxy cement. The metal surfaces were coated with waterproof nail varnish (an electrical insulator), and a circle of vacuum grease (also an electrical insulator) was drawn around the electrode to make a well in which ACSF could be held. The stimulating electrode was positioned to stimulate Schaffer collaterals in the stratum radiatum of CA1 and secured in place on top of the array by nylon strings attached to a loop of platinum wire. The recording electrode (final resistance $\approx$5 MΩ) was pulled from a borosilicate glass capillary (1.5 mm outer diameter, 0.84 mm inner diameter; World Precision Instruments) and filled with a patch clamp electrolyte consisting of CsCl 140 mM, 4-(2-hydroxyethyl)-1-piperazineethanesulfonic acid (HEPES) 5 mM, ethylene glycol tetraacetic acid (EGTA) 10 mM, Mg-adenosine triphosphate (Mg-ATP) 2 mM, pH 7.4, $\approx$295 mOsm L^{-1} and whole-cell voltage clamp recordings were then made according to standard methods.[120] The patch clamp setup consisted of an EPC9/2 patch clamp amplifier (HEKA Elektronik Dr. Schulze GmbH, Lambrecht/Pfalz Germany) connected via the built-in ITC-16 digitizer board to a computer running Pulse software (version 8.80, HEKA); currents were amplified 10×, sequentially low-pass filtered at 10 kHz then 3 kHz and digitized at 10 kHz. Stimulation was controlled within the Pulse software and delivered via a Grass SD9 constant voltage stimulator (10 V × 80 μs). All recordings were made in the presence of 6 μM gabazine (HelloBio, UK), an antagonist of type A γ-aminobutyric acid (GABA) receptors, to isolate excitatory postsynaptic currents. The α-amino-3-hydroxy-5-methyl-4-isoxazolepropionic (AMPA) and kainate subtypes of glutamate receptors were blocked by bath application of 6-cyano-7-nitroquinoxaline-2,3-dione (CNQX; Tocris, UK).

Printing in SMPs: Optically transparent shape-memory polyimide (TSMPI) was prepared by adaptation of the literature[95] to include a doctor blade step to deposit films of $\approx$40 μm in thickness on glass slides. Structures were printed using an ink formulation (composed of pyrrole (50 μL, purified by passage over basic alumina), ethanol (950 μL), irgacure D-2959 (10 mol % concentration relative to pyrrole)) with laser writing powers of $\approx$80–100%, followed by ethanol washing, yielding structures depicted in Figure S6, Supporting Information.

Ink Formulation for 3D Printing In Vivo: Pyrrole (1 mL, purified by passage over basic alumina), irgacure D-2959 (50 mg), PEG (10 kDa, 1 mg), PEGDMA (2 kDa, 1 mg), and hyaluronic acid (50 mg). The inks were sonicated for $\approx$25 min in the dark at room temperature to ensure mixing and left to rest for $\approx$25 min in the dark for any insoluble material to settle, after which the clear upper layer (saturated with monomer, initiator, and dopant) was either used for toxicity screening (death

**ADVANCED
SCIENCE NEWS**

www.advancedsciencenews.com

**ADVANCED
MATERIALS
TECHNOLOGIES**

www.advmattechnol.de

fluorescence,[109] or bioluminescence developmental assays)[110] or mixed with *E. coli* OP50 bacterial paste and used for printing either in PDMS (as described above) or *C. elegans* (as described below).

Elegans Acute Adult Toxicity Testing: Worms were synchronized by bleaching and raised at 20 °C on *E. coli* OP50-seeded nematode-growth medium plates as previously described[121] until they reached the L4 stage. L4 worms were then transferred to new *E. coli* OP50-seeded nematode-growth medium plates at 25 °C for 24 h before processing them for survival assays. Photoresist component stock solutions in dimethylsulfoxide (DMSO) were diluted serially in M9 buffer to yield the concentrations tested. Assays were run and analyzed as previously described,[108] substituting the oxidant *t*-BHP with the photoresist component solutions.

Elegans Developmental Toxicity Testing: Worms were synchronized by bleaching and raised at 20 °C on *E. coli* OP50-seeded nematode-growth medium plates as previously described.[121] To assess chronic developmental toxicity, synchronized L1 worms were collected in sterile M9 buffer, washed three times in M9, and the worm concentration of the resulting solution was determined by counting the number of worms in four 10 µL drops of the solution under a stereomicroscope at 40× magnification. Photoresist component stock solutions in DMSO were diluted serially in M9 buffer to yield the concentrations tested. The developmental assay was adapted from Olmedo et al.[110] Briefly, ≈20 worms per well and a 2–3 µL bacterial pellet were dispensed in 30 µL of M9 in each well of a 384-well white microplate. Following dispensing of worms and bacteria in all wells, 8 µL of each test solution and 40 µL of 2× luciferin solution (for final concentration see literature)[110] were added to each well. Bioluminescence measurements were carried out every 6 min as described[110] for up to 72 h in a Tecan Infinite M200 Pro (Tecan Ltd.). Readouts were plotted and analyzed blind in Microsoft Excel 365 to determine the timings and lengths of larval stages. Statistics performed used two-way analysis of variance (ANOVA) with post-hoc Dunnett's correction for multiple comparisons.

PDMS Groove Preparation for 3D-Printing on C. elegans: To trap worms while printing onto or inside them, a thermally resilient and optically clear matrix is needed. The 2–4% agarose pads used in traditional setups for *C. elegans* microscopy observations were thus substituted for 75 µm thin PDMS films. PDMS (Sylgard 184, Farnell) at 14:1 base to curing agent ratio was spin-coated at 700 rpm on 12-inch vinyl record chunks (typically 2–3 inches wide) for 1 min, baked at 60 °C for 3 h, cut in 1 cm² slabs, and bound to 22 and 30 mm diameter coverslips using oxygen plasma activation of silicon surfaces. Coated coverslips were stored in a dust-free environment until use. Before use, they were briefly rinsed with isopropanol and dried with an air gun.

Printing In Vivo in C. elegans: Wildtype *C. elegans* Bristol N2 worms were maintained as previously described.[121] Synchronized day 1-old adult worms were then fed a 1:5 mixture of ink/photoresist and concentrated *E. coli* OP50 bacterial paste (100 times concentrated from an OD_{600} nm = 1 solution in lysogenic broth) dispensed and spread (after homogenization by vortexing 20 s following a 30 min incubation at 30 °C) at 200 µL per 6 cm Nematode Growth Medium Agar plate, for 1 h at 25 °C. Worms were then immobilized in 0.2% levamisole prepared in a 2 µL drop of an even mix of 1:10 mixture of photoresist and concentrated OP50 and M9 medium, between two 1 cm² slabs of PDMS grooves bonded onto a 22 mm-diameter and 30 mm-diameter coverslips (PDMS film were prepared by spin-coating at 700 rpm on vinyl records for 1 min, baked at 60 °C for 3 h, cut in 1 cm² slabs, and bound to coverslips by plasma-cleaning). During worm mounting, worms were aligned inside the grooves using a platinum pick, and vacuum grease was used to seal the edges of the coverslips. Coverslips were then mounted into the Nanoscribe holder (Herma glue was dotted around the edges of the coverslip binding it to the holder and left to dry for 10 min) and a drop of immersion oil (Immersol 518F) was applied. The sample was then processed for 3D nano-printing through a Zeiss 63 × 1.4NA lens from a Nanoscribe Photonic Professional GT 700 instrument operating in galvo mode at speeds of 500–1000 µm s⁻¹ with a laser power output of 40–60 mW (Topica FemtoFiber pro-Er-doped fiber laser with a pulse duration < 150 fs, a repetition rate of 100 MHz, a wavelength of 780 nm, an aperture of 7.3 mm and a diode voltage of 1.34–5).

Confocal Imaging of C. elegans: Following 3D printing, worms were collected by transferring the coverslips onto a microscopy slide with M9 added to prevent desiccation. The slides were then imaged through a Zeiss 40 × 1.4NA oil immersion lens with a Zeiss LSM880 confocal microscope exciting the sample at 488 nm and collecting fluorescence signal at 543 nm and operated by the Zen Black software. Z-stacks were acquired at 1024 × 1024 pixels[2] every 0.45 µm across the first half of the worm thickness (about 30 µm). single plane sequences were acquired at maximum speed (1.5 s per frame after averaging). Images were then exported and processed with FiJi for figure preparation.[122]

Supporting Information

Supporting Information is available from the Wiley Online Library or from the author.

Conflict of Interest

J.G.H. is inventor of: Photoinitiating polymerisable composition. PCT/GB2017/052235, EP3493859A1, GB2562443A, GB2562443B, US20190175796A1, WO2018025026A1.

Author Contributions

P.K., G.R.H., and R.G. contributed equally to this work. Conceptualization, J.G.H.; methodology, all authors; formal analysis, all authors; investigation, S.J.B., P.K., G.R.H., R.G., H.H.G., M.J.F., Zh.Z., Zi.Z., J.R.M., C.A., M.D.A., M.J.H., B.S., D.C., D.M.C., and A.B.;

Data Availability Statement

The data that support the findings of this study are available on request from the corresponding author. The data are not publicly available due to privacy or ethical restrictions.

Keywords

[1] C. Tulkoff, G. Caswell, *Design for Excellence in Electronics Manufacturing*, Wiley, New York **2021**.

[2] H. Cagnan, T. Denison, C. Mcintyre, P. Brown, *Nat. Biotechnol.* **2019**, *37*, 1024.

[3] Y. Cho, S. Park, J. Lee, K.i J. Yu, *Adv. Mater.* **2021**, *33*, 2005786.

[4] A. Fanelli, L. Ferlauto, E. G. Zollinger, O. Brina, P. Reymond, P. Machi, D. Ghezzi, *Adv. Mater. Technol.* **2022**, *7*, 2100176.

[5] J. A. Frank, M.-J. Antonini, P. Anikeeva, *Nat. Biotechnol.* **2019**, *37*, 1013.

[6] S. G. Higgins, I. Lo Fiego, I. Patrick, A. Creamer, M. M. Stevens, *Adv. Mater. Technol.* **2020**, *5*, 2000384.

[7] D. C. Kim, H. J. Shim, W. Lee, J.a H. Koo, D.-H. Kim, *Adv. Mater.* **2020**, *32*, 2070118.

[8] Y. Liu, V. R. Feig, Z. Bao, *Adv. Healthcare Mater.* **2021**, *10*, 2001916.

[9] L. Luan, J. T. Robinson, B. Aazhang, T. Chi, K. Yang, X. Li, H. Rathore, A. Singer, S. Yellapantula, Y. Fan, Z. Yu, C. Xie, *Neuron* **2020**, *108*, 302.

[10] S. R. Patel, C. M. Lieber, *Nat. Biotechnol.* **2019**, *37*, 1007.

[11] A. E. Rochford, A. Carnicer-Lombarte, V. F. Curto, G. G. Malliaras, D. G. Barone, *Adv. Mater.* **2020**, *32*, 1903182.

[12] D. Shahriari, D. Rosenfeld, P. Anikeeva, *Neuron* **2020**, *108*, 270.

[13] A. Singer, J. T. Robinson, *Adv. Healthcare Mater.* **2021**, *10*, 2100664.

[14] J.-Y. Yoo, J.-S. Yang, M.-K. Chung, S.-H.o Kim, J.-B.o Yoon, *J. Micromech. Microeng.* **2021**, *31*, 074001.

[15] S. Yoo, J. Lee, H. Joo, S.-H. Sunwoo, S. Kim, D.-H. Kim, *Adv. Healthcare Mater.* **2021**, *10*, 2100614.

[16] Q.i Zeng, X. Li, S. Zhang, C. Deng, T. Wu, *Nano Sel.* **2022**, *3*, 903.

[17] M. Zhang, Z. Tang, X. Liu, J. Van Der Spiegel, *Nat. Electron.* **2020**, *3*, 191.

[18] M. Zou, Y. Ma, X. Yuan, Y.i Hu, J. Liu, Z. Jin, *J. Semicond.* **2018**, *39*, 011010.

[19] O. Bettucci, G. M. Matrone, F. Santoro, *Adv. Mater. Technol.* **2022**, *7*, 2100293.

[20] J. Marques-Hueso, T. D. A. Jones, D. E. Watson, A. Ryspayeva, M. N. Esfahani, M. P. Shuttleworth, R. A. Harris, R. W. Kay, M. P. Y. Desmulliez, *Adv. Funct. Mater.* **2018**, *28*, 1704451.

[21] R. N. Esfahani, M. P. Shuttleworth, V. Doychinov, N. J. Wilkinson, J. Hinton, T. D. A. Jones, A. Ryspayeva, I. D. Robertson, J. Marques-Hueso, M. P. Y. Desmulliez, R. A. Harris, R. W. Kay, *Addit. Manuf.* **2020**, *34*, 101367.

[22] A. Ryspayeva, T. D. A. Jones, M. N. Esfahani, M. P. Shuttleworth, R. A. Harris, R. W. Kay, M. P. Y. Desmulliez, J. Marques-Hueso, *Microelectron. Eng.* **2019**, *209*, 35.

[23] E. Manousiouthakis, J. Park, J. G. Hardy, J. Y. Lee, C. E. Schmidt, *Acta Biomater.* **2022**, *139*, 22.

[24] T. Someya, Z. Bao, G. G. Malliaras, *Nature* **2016**, *540*, 379.

[25] X. Guo, M. Baumgarten, K. Müllen, *Prog. Polym. Sci.* **2013**, *38*, 1832.

[26] T. Nezakati, A. Seifalian, A. Tan, A. M. Seifalian, *Chem. Rev.* **2018**, *118*, 6766.

[27] Y. Chen, Y. Zhang, Z. Liang, Y.u Cao, Z. Han, X. Feng, *npj Flexible Electron.* **2020**, *4*, 2.

[28] L. Guo, M. Ma, N. Zhang, R. Langer, D. G. Anderson, *Adv. Mater.* **2014**, *26*, 1427.

[29] H.-L. Park, Y. Lee, N. Kim, D.-G. Seo, G.-T. Go, T.-W. Lee, *Adv. Mater.* **2020**, *32*, 1903558.

[30] E. Song, J. Li, S. M. Won, W. Bai, J. A. Rogers, *Nat. Mater.* **2020**, *19*, 590.

[31] E. A. Cuttaz, C. A. R. Chapman, O. Syed, J. A. Goding, R. A. Green, *Adv. Sci.* **2021**, *8*, 2004033.

[32] Q. Yang, T. Wei, R. T. Yin, M. Wu, Y. Xu, J. Koo, Y. S. Choi, Z. Xie, S. W. Chen, I. Kandela, S. Yao, Y. Deng, R. Avila, T.-L.i Liu, W. Bai, Y. Yang, M. Han, Q. Zhang, C. R. Haney, K. Benjamin Lee, K. Aras, T. Wang, M.-H.o Seo, H. Luan, S. M. Lee, A. Brikha, N. Ghoreishi-Haack, L. Tran, I. Stepien, F. Aird, et al., *Nat. Mater.* **2021**, *20*, 1559.

[33] G. L. Goh, H. Zhang, T. H. Chong, W. Y. Yeong, *Adv. Electron. Mater.* **2021**, *7*, 2100445.

[34] M. Layani, X. Wang, S. Magdassi, *Adv. Mater.* **2018**, *30*, 1706344.

[35] H. Yuk, B. Lu, S. Lin, K. Qu, J. Xu, J. Luo, X. Zhao, *Nat. Commun.* **2020**, *11*, 1604.

[36] A. Piqué, B. Pratap, S. A. Mathews, B. J. Karns, R. C. Auyeung, M. Kasser, M. Ollinger, H. Kim, S. Lakeou, C. B. Arnold, *Proc. SPIE* **2005**, *5713*, 223.

[37] O. Dadras-Toussi, M. Khorrami, A. S. C. Louis Sam Titus, S. Majd, C. Mohan, M. R. Abidian, *Adv. Mater.* **2022**, *34*, 2200512.

[38] L. Li, J. T. Fourkas, *Mater. Today* **2007**, *10*, 30.

[39] A. K. Nguyen, R. J. Narayan, *Mater. Today Bio* **2017**, *20*, 314.

[40] T. Wloka, M. Gottschaldt, U. S. Schubert, *Chemistry* **2022**, *28*, 202104191.

[41] J. G. Hardy, D. S. Hernandez, D. M. Cummings, F. A. Edwards, J. B. Shear, C. E. Schmidt, *J. Mater. Chem. B* **2015**, *3*, 5001.

[42] J. G. Hardy, M. Palma, S. J. Wind, M. J. Biggs, *Adv. Mater.* **2016**, *28*, 5717.

[43] J. A. Goding, A. D. Gilmour, U. A. Aregueta-Robles, E. A. Hasan, R. A. Green, *Adv. Funct. Mater.* **2018**, *28*, 1702969.

[44] A. Novikov, J. Goding, C. Chapman, E. Cuttaz, R. A. Green, *APL Mater.* **2020**, *8*, 101105.

[45] N. Adly, S. Weidlich, S. Seyock, F. Brings, A. Yakushenko, A. Offenhäusser, B. Wolfrum, *npj Flexible Electron.* **2018**, *2*, 15.

[46] A. Bohr, K. Memarzadeh, *Artificial Intelligence in Healthcare* (Eds: A. Bohr, K. Memarzadeh), Academic Press, Boca Raton, FL **2020**, pp. 25–60.

[47] A. C. Chang, *Intelligence-Based Medicine: Artificial Intelligence and Human Cognition in Clinical Medicine and Healthcare* (Ed: A. C. Chang), Academic Press, Boca Raton, FL **2020**, pp. 431–443.

[48] L. Drew, *Nature* **2019**, *571*, S19.

[49] P. Shah, F. Kendall, S. Khozin, R. Goosen, J. Hu, J. Laramie, M. Ringel, N. Schork, *npj Digital Med.* **2019**, *2*, 69.

[50] P. K. R. Maddikunta, Q.-V. Pham, P. B, N. Deepa, K. Dev, T. R. Gadekallu, R. Ruby, M. Liyanage, *J. Ind. Inf. Integr.* **2022**, *26*, 100257.

[51] K.j Manjunatheshwara, S. Vinodh, *Int. J. Sustainable Eng.* **2021**, *14*, 541.

[52] L. Wang, *J. Manuf. Syst.* **2022**, *62*, 199.

[53] K. T. Butler, D. W. Davies, H. Cartwright, O. Isayev, A. Walsh, *Nature* **2018**, *559*, 547.

[54] J. G. Hardy, S. Sdepanian, A. F. Stowell, A. D. Aljohani, M. J. Allen, A. Anwar, D. Barton, J. V. Baum, D. Bird, A. Blaney, L. Brewster, D. Cheneler, O. Efremova, M. Entwistle, R. N. Esfahani, M. Firlak, A. Foito, L. Forciniti, S. A. Geissler, F. Guo, R. M. Hathout, R. Jiang, P. Kevin, D. Leese, W. L.i Low, S. Mayes, M. Mozafari, S. T. Murphy, H. Nguyen, C. N. M. Ntola, et al., *J. Chem. Educ.* **2021**, *98*, 1124.

[55] J. J. De Pablo, N. E. Jackson, M. A. Webb, L.-Q. Chen, J. E. Moore, D. Morgan, R. Jacobs, T. Pollock, D. G. Schlom, E. S. Toberer, J. Analytis, I. Dabo, D. M. Delongchamp, G. A. Fiete, G. M. Grason, G. Hautier, Y. Mo, K. Rajan, E. J. Reed, E. Rodriguez, V. Stevanovic, J. Suntivich, K. Thornton, J.-C. Zhao, *npj Comput. Mater.* **2019**, *5*, 41.

[56] Y. Liu, C. Niu, Z. Wang, Y. Gan, Y. Zhu, S. Sun, T. Shen, *J. Mater. Sci. Technol.* **2020**, *57*, 113.

[57] M. N. Helmus, D. F. Gibbons, D. Cebon, *Toxicol. Pathol.* **2008**, *36*, 70.

[58] S. Lueddeckens, P. Saling, E. Guenther, *Int. J. Life Cycle Assess.* **2020**, *25*, 1385.

[59] P. Ramesh, S. Vinodh, *Int. J. Sustainable Eng.* **2020**, *13*, 411.

[60] C. A. Marchant, *Wiley Interdiscip. Rev.: Comput. Mol. Sci.* **2012**, *2*, 424.

[61] J. Hemmerich, G. F. Ecker, *Wiley Interdiscip. Rev.: Comput. Mol. Sci.* **2020**, *10*, 1475.

[62] A. B. Raies, V. B. Bajic, *Wiley Interdiscip. Rev.: Comput. Mol. Sci.* **2016**, *6*, 147.

[63] A. B. Raies, V. B. Bajic, *Wiley Interdiscip. Rev.: Comput. Mol. Sci.* **2018**, *8*, 1352.

[64] R. H. In, *Front. Pharmacol.* **2011**, *2*, 33.

[65] K.-T. Rim, *Toxicol. Environ. Health Sci.* **2020**, *12*, 191.

[66] E. Pérez Santín, R. Rodríguez Solana, M. González García, M. D. Mar García Suárez, G. D. Blanco Díaz, M. D. Cima Cabal, J. M. Moreno Rojas, J. I. López Sánchez, *Wiley Interdiscip. Rev.: Comput. Mol. Sci.* **2021**, *11*, 1516.

[67] J. Tropp, J. Rivnay, *J. Mater. Chem. C* **2021**, *9*, 13543.

[68] E. Hodgson, P. E. Levi, *A Textbook of Modern Toxicology*, Elsevier, New York **1987**.

[69] K. A. Ford, *ILAR J.* **2016**, *57*, 226.

[70] J. C. Madden, S. J. Enoch, A. Paini, M. T. D. Cronin, *Altern. Lab. Anim.* **2020**, *48*, 146.

[71] E. Törnqvist, A. Annas, B. Granath, E. Jalkesten, I. Cotgreave, M. Öberg, *PLoS One* **2014**, *9*, 101638.

[72] M. D. Ashton, I. C. Appen, M. Firlak, N. E. Stanhope, C. E. Schmidt, W. R. Eisenstadt, B. Hur, J. G. Hardy, *Polym. Int.* **2021**, *70*, 467.

[73] T. Distler, C. Polley, F. Shi, D. Schneidereit, M. D. Ashton, O. Friedrich, J. F. Kolb, J. G. Hardy, R. Detsch, H. Seitz, A. R. Boccaccini, *Adv. Healthcare Mater.* **2021**, *10*, 2001876.

[74] A. Magaz, M. D. Ashton, R. M. Hathout, X.u Li, J. G. Hardy, J. J. Blaker, *Pharmaceutics* **2020**, *12*, 742.

[75] A. V. Edwards, C. Hann, H. Ivill, H. Leeson, L. Tymczyszyn, D. M. Cummings, M. D. Ashton, G. R. Harper, D. T. Spencer, W. L.i Low, K. Rajeev, P. Martin-Hirsch, F. A. Edwards, J. G. Hardy, A. E. W. Rennie, D. Cheneler, *Mater. Adv.* **2021**, *2*, 1600.

[76] D. Qi, K. Zhang, G. Tian, B.o Jiang, Y. Huang, *Adv. Mater.* **2021**, *33*, 2003155.

[77] Y. N. Ertas, D. Ozpolat, S. N. Karasu, N. Ashammakhi, *Micromachines* **2022**, *13*, 1081.

[78] M. B. Gluth, R. Singh, M. D. Atlas, *Cochlear Implants Int.* **2011**, *12*, 223.

[79] M. Copeland, M. Choi, I. J. Bleiweiss, *Plast. Reconstr. Surg.* **1994**, *94*, 643.

[80] S. G. Haider, O. Stuhl, H. G. Goslar, L. Birkofer, *Cell. Mol. Biol.* **1983**, *29*, 299.

[81] C. Rücker, K. Kümmerer, *Chem. Rev.* **2015**, *115*, 466.

[82] P. Kaali, D. Momcilovic, A. Markström, R. Aune, G. Czel, S. Karlsson, *J. Appl. Polym. Sci.* **2010**, *115*, 802.

[83] M. Tohfafarosh, A. Sevit, J. Patel, J. W. Kiel, A. Greenspon, J. M. Prutkin, S. M. Kurtz, *J. Long-Term Eff. Med. Implants* **2016**, *26*, 225.

[84] J. Jeong, N. Chou, S. Kim, *Biomed. Microdevices* **2016**, *18*, 42.

[85] T. Senzaki, S. Fujikawa, *Chem. Lett.* **2019**, *48*, 1152.

[86] H. Zhang, M. Chiao, *J. Med. Biol. Eng.* **2015**, *35*, 143.

[87] S. Au-Yong, M. Firlak, E. R. Draper, S. Municoy, M. D. Ashton, G. R. Akien, N. R. Halcovitch, S. J. Baldock, P. Martin-Hirsch, M. F. Desimone, J. G. Hardy, *Polymers* **2022**, *14*, 4953.

[88] M. Elbohouty, M. T. Wilson, L. J. Voss, D. A. Steyn-Ross, L. A. Hunt, *Phys. Med. Biol.* **2013**, *58*, 3599.

[89] K. Fidanovski, D. Mawad, *Adv. Healthcare Mater.* **2019**, *8*, 1900053.

[90] W. F. Gillis, C. A. Lissandrello, J. Shen, B. W. Pearre, A. Mertiri, F. Deku, S. Cogan, B. J. Holinski, D. J. Chew, A. E. White, T. M. Otchy, T. J. Gardner, *J. Neural Eng.* **2018**, *15*, 016010.

[91] M. J. Haskew, J. G. Hardy, *Johnson Matthey Technol. Rev.* **2020**, *64*, 425.

[92] H. Lee, Y. Won, J. H. Oh, *J. Polymer Sci.* **2022**, *60*, 348.

[93] Y. Liang, A. Offenhäusser, S. Ingebrandt, D. Mayer, *Adv. Healthcare Mater.* **2021**, *10*, 2100061.

[94] C. A. Lissandrello, W. F. Gillis, J. Shen, B. W. Pearre, F. Vitale, M. Pasquali, B. J. Holinski, D. J. Chew, A. E. White, T. J. Gardner, *J. Neural Eng.* **2017**, *14*, 036006.

[95] X. Xiao, X. Qiu, D. Kong, W. Zhang, Y. Liu, J. Leng, *Soft Matter* **2016**, *12*, 2894.

[96] S. M. Richardson-Burns, J. L. Hendricks, B. Foster, L. K. Povlich, D.-H. Kim, D. C. Martin, *Biomaterials* **2007**, *28*, 1539.

[97] D. Parker, Y. Daguerre, G. Dufil, D. Mantione, E. Solano, E. Cloutet, G. Hadziioannou, T. Näsholm, M. Berggren, E. Pavlopoulou, E. Stavrinidou, *Mater. Horiz.* **2021**, *8*, 3295.

[98] D. Parker, Y. Daguerre, G. Dufil, D. Mantione, E. Solano, E. Cloutet, G. Hadziioannou, T. Näsholm, M. Berggren, E. Pavlopoulou, E. Stavrinidou, *Mater. Horiz.* **2022**, *9*, 1317.

[99] E. Stavrinidou, R. Gabrielsson, K. P. R. Nilsson, S. K. Singh, J. F. Franco-Gonzalez, A. V. Volkov, M. P. Jonsson, A. Grimoldi, M. Elgland, I. V. Zozoulenko, D. T. Simon, M. Berggren, *Proc. Natl. Acad. Sci. U. S. A.* **2017**, *114*, 2807.

[100] G. Tommasini, G. Dufil, F. Fardella, X. Strakosas, E. Fergola, T. Abrahamsson, D. Bliman, R. Olsson, M. Berggren, A. Tino, E. Stavrinidou, C. Tortiglione, *Bioact. Mater.* **2022**, *10*, 107.

[101] H. A. Galeb, E. L. Wilkinson, A. F. Stowell, H. Lin, S. T. Murphy, P. L. Martin-Hirsch, R. L. Mort, A. M. Taylor, J. G. Hardy, *Global Challenges* **2021**, *5*, 2000102.

[102] A. Ovsianikov, S. Mühleder, J. Torgersen, Z. Li, X.-H. Qin, S. Van Vlierberghe, P. Dubruel, W. Holnthoner, H. Redl, R. Liska, J. Stampfl, *Langmuir* **2014**, *30*, 3787.

[103] J. Torgersen, A. Ovsianikov, V. Mironov, N. Pucher, X. Qin, Z. Li, K. Cicha, T. Machacek, R. Liska, V. Jantsch, J. Stampfl, *J. Biomed. Opt.* **2012**, *17*, 105008.

[104] Y. Liu, J. Li, S. Song, J. Kang, Y. Tsao, S. Chen, V. Mottini, K. Mcconnell, W. Xu, Y.u-Q. Zheng, J. B.-H. Tok, P. M. George, Z. Bao, *Nat. Biotechnol.* **2020**, *38*, 1031.

[105] J. G. Hardy, EP3493859A1 **2019**.

[106] A. Urciuolo, I. Poli, L. Brandolino, P. Raffa, V. Scattolini, C. Laterza, G. G. Giobbe, E. Zambaiti, G. Selmin, M. Magnussen, L. Brigo, P. De Coppi, S. Salmaso, M. Giomo, N. Elvassore, *Nat. Biomed. Eng.* **2020**, *4*, 901.

[107] Y. Chen, J. Zhang, X. Liu, S. Wang, J. Tao, Y. Huang, W. Wu, Y. Li, K. Zhou, X. Wei, S. Chen, X. Li, X. Xu, L. Cardon, Z. Qian, M. Gou, *Sci. Adv. 6*, aba7406.

**ADVANCED
SCIENCE NEWS**

www.advancedsciencenews.com

**ADVANCED
MATERIALS
TECHNOLOGIES**

www.advmattechnol.de

[108] A. Benedetto, T. Bambade, C. Au, J. M. A. Tullet, J. Monkhouse, H. Dang, K. Cetnar, B. Chan, F. Cabreiro, D. Gems, *Aging Cell* **2019**, *18*, 12998.

[109] C. Coburn, E. Allman, P. Mahanti, A. Benedetto, F. Cabreiro, Z. Pincus, F. Matthijssens, C. Araiz, A. Mandel, M. Vlachos, S.-A. Edwards, G. Fischer, A. Davidson, R. E. Pryor, A. Stevens, F. J. Slack, N. Tavernarakis, B. P. Braeckman, F. C. Schroeder, K. Nehrke, D. Gems, *PLoS Biol.* **2013**, *11*, 1001613.

[110] M. Olmedo, M. Geibel, M. Artal-Sanz, M. Merrow, *Genetics* **2015**, *201*, 443.

[111] S. Miller, M. J. Selgelid, *Sci. Eng. Ethics* **2007**, *13*, 523.

[112] I. Jarchum, *Nat. Biotechnol.* **2019**, *37*, 993.

[113] G. Laurie, *Novel Neurotechnologies: Intervening on the Brain*, Edinburgh Research Explorer, Edinburgh **2014**.

[114] S. M. Pfotenhauer, N. Frahm, D. Winickoff, D. Benrimoh, J. Illes, G. Marchant, *Nat. Biotechnol.* **2021**, *39*, 661.

[115] S. Lawman, Y. Dong, B. M. Williams, V. Romano, S. Kaye, S. P. Harding, C. Willoughby, Y.-C. Shen, Y. Zheng, *Opt. Express* **2016**, *24*, 12395.

[116] Y. Dong, H. Lin, V. Abolghasemi, L.u Gan, J. A. Zeitler, Y.-C. Shen, *J. Pharm. Sci.* **2017**, *106*, 546.

[117] H. Lin, Z. Zhang, D. Markl, J. Zeitler, Y. Shen, *Appl. Sci.* **2018**, *8*, 2700.

[118] Z. Zhang, U. Ikpatt, S. Lawman, B. Williams, Y. Zheng, H. Lin, Y. Shen, *Opt. Express* **2019**, *27*, 13951.

[119] A. C. M. Kuo, in *Polymer Data Handbook* (Ed: J. E. Mark), Oxford University Press, New York **1999**, pp. 411–435.

[120] D. P. Benitez, S. Jiang, J. Wood, R. Wang, C. M. Hall, C. Peerboom, N. Wong, K. M. Stringer, K. S. Vitanova, V. C. Smith, D. Joshi, T. Saito, T. C. Saido, J. Hardy, J. Hanrieder, B. De Strooper, D. A. Salih, T. Tripathi, F. A. Edwards, D. M. Cummings, *Mol. Neurodegener.* **2021**, *16*, 47.

[121] T. Stiernagle, in *WormBook: The Online Review of C. elegans Biology* (Ed: The C. elegans Research Community), WormBook, Pasadena, CA **2006**, pp. 1551–8507.

[122] R. Lima, D. Sousa, A. Paiva, A. Palmeira, J. Barbosa, M. Pedro, M. Pinto, E. Sousa, M. Vasconcelos, *Molecules* **2016**, *21*, 1343.